Eur. Phys. J. A (2016) **52**: 77
DOI 10.1140/epja/i2016-16077-2

THE EUROPEAN PHYSICAL JOURNAL A

Review

Nuclear astrophysics and the Trojan Horse Method*

C. Spitaleri[1,2,a], M. La Cognata[2], L. Lamia[1], A.M. Mukhamedzhanov[3], and R.G. Pizzone[2]

[1] Dipartimento di Fisica e Astronomia, University of Catania, via S. Sofia 64, 95123 Catania, Italy
[2] Laboratori Nazionali del Sud - INFN, via S. Sofia 62, 95123 Catania, Italy
[3] Cyclotron Institute, Texas A&M University, College Station, TX 77843, USA

Received: 3 July 2015 / Revised: 23 September 2015
Published online: 5 April 2016 –
Communicated by C. Broggini

Abstract. In this review, we discuss the new recent results of the Trojan Horse Method that is used to determine reaction rates for nuclear processes in several astrophysical scenarios. The theory behind this technique is shortly presented. This is followed by an overview of some new experiments that have been carried out using this indirect approach.

1 Introduction

The production of energy in the stars and element formation in the Universe are among the main goals of nuclear physics and astrophysics. It would not be possible to understand what is the evolution of stars and their life cycle without the knowledge of stellar nucleosynthesis [1–4]. Fusion of charged particles occurs at the so-called *Gamow energy* (E_G), usually much lower than the Coulomb barrier under stellar quiescent burning conditions. Typically, E_G is of the order of keV while the Coulomb barrier E_C of the interacting nuclei is of order of MeV. The Coulomb barrier often makes the cross section $\sigma_b(E)$ of the reactions too small to measure since $\sigma_b(E)$ drops exponentially with decreasing energy. Thus, direct measurements of $\sigma_b(E)$ exhibit a low-energy limit, usually at energies much larger than E_G. Extrapolation from measurements at higher energies would be the standard way to obtain $\sigma_b(E)$, but extrapolation is complicated because of the exponential variation of the cross section $\sigma_b(E)$, entailing the occurrence of many possible sources of systematic errors. The astrophysical factor $S(E)$ was then adopted as a way to characterize cross sections by removing the gross contribution of the Coulomb penetration factor, since it shows a much weaker energy dependence than the cross section $\sigma_b(E)$. However, such an extrapolation into the unknown can lead to considerable uncertainties and important contributions to the excitation functions, like resonance tails of sub-threshold resonances, can be missed [3,4].

In those cases where accurate direct measurements come within, or close to, the Gamow peak (*e.g.*, [5]), an unexpected effect shows up, attributed to the presence of atomic electrons [6]. Electron clouds are responsible for the increase of the cross section at low energies with respect to the case of bare nuclei (whence the subscript b used so far to characterize cross sections), the so-called *electron screening* effect [6,7]. To parameterize such increment due to the screening effect, an *enhancement factor* $f_{\rm lab}$ is usually introduced, defined as

$$f_{\rm lab}(E) = \sigma_s(E)/\sigma_b(E) \sim \exp[\pi\eta(U_e/E)], \qquad (1)$$

where U_e is the electron screening potential, η the Sommerfeld parameter and the subscript s is used for the screened cross section. Electron screening is more important, the closer the interaction energies are to the electron screening potential, being the enhancement not negligible already at $E/U_e \sim 100$ [6]. Typical values of U_e are given, for instance, in ref. [6] and equal $\sim 30\,\text{eV}$ for the $d+d$ system and $\sim 6\,\text{keV}$ in the case of the $^{12}\text{C} + {}^{12}\text{C}$ interaction. Therefore, electron screening is usually not negligible in quiescent stellar burning while in higher temperature environments, such as supernovae, it can be neglected. Since $S(E_G)$ for bare nuclei is not available experimentally, extrapolation is needed even when measured cross sections are available in the Gamow energy range.

Electron screening is an additional challenge for direct measurements at the low energies necessary to astrophysics. To overcome the experimental difficulties of direct measurements, a number of indirect methods have been suggested to measure bare nucleus cross sections at low energies. Several indirect methods such as Coulomb Dissociation [8], Asymptotic Normalization Coefficient [9, 10], and Trojan Horse Method (THM) [11–19] have been

* Contribution to the Topical Issue "Underground nuclear astrophysics and solar neutrinos: Impact on astrophysics, solar and neutrino physic" edited by Gianpaolo Bellini, Carlo Broggini, Alessandra Guglielmetti.

[a] e-mail: spitaleri@lns.infn.it

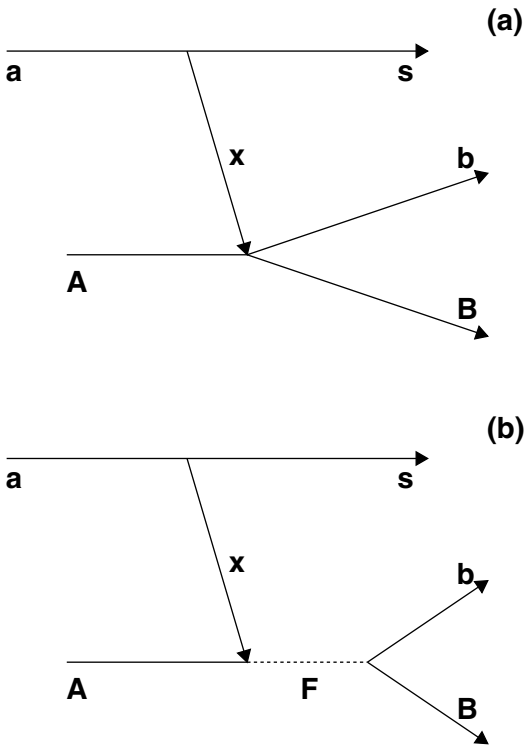

Fig. 1. Diagrams describing the TH reaction $a+A \rightarrow b+B+s$ in the QF kinematics, proceeding through the direct $x+A \rightarrow b+B$ sub-reaction (a) or through the formation of the $F = b+B$ resonant state (b).

developed in the last 25 years. In indirect techniques, nuclear reaction theory is necessary to link the cross section of the measured process to the one of the astrophysical reaction of interest.

In this paper we address only the THM, which provides a way to determine the reaction rate for reactions having hadrons in the exit channel [11,18,19]. Throughout this work, we will assume $\hbar = c = 1$.

2 Trojan Horse Method: Generalities

The THM is an extension of quasi-free (QF) reaction mechanism studies [20–24] to low incident energies ($\leq$ 70 MeV) [12,25–27].

The THM, first suggested by Baur [11], aims at obtaining the cross section of the binary process $x + A \rightarrow b + B$ at astrophysical energies by measuring the cross section of a $a + A \rightarrow b + B + s$ THM reaction in the QF kinematic regime. Under these conditions, the TH particle a, which has a dominant s-x cluster structure, is accelerated at energies above the Coulomb barrier and, after penetrating the barrier, undergoes breakup in the nuclear field of A. There, x interacts with A while s, also called the *spectator*, flies away. From the measured three-body cross section, the energy dependence of the binary sub-process $x + A \rightarrow b + B$ is determined. The QF reaction used to extract the $x + A \rightarrow b + B$ cross section is schematically shown in fig. 1, in the case of direct (a) or resonant (b) sub-reactions. Since the projectile energy is chosen larger than the A-a Coulomb barrier E_C^{aA}, the probability to find a near A, which is given by the square modulus of the scattering wave function describing their relative motion, is not suppressed [28], leading to a finite probability that A can be in the proximity of x. This is an heuristic explanation of the possibility to explore the whole Gamow window by using the THM, with no need of extrapolation. A more detailed explanation takes into account the virtual nature of the transferred particle x, whose energy and momentum are not related by the (non-relativistic) mass-shell equation $E_x = {k_x}^2/2m_x$. Therefore, as we will see in the forthcoming sections, corrections have to be introduced to account for off-energy-shell effects (see ref. [19] and references therein for details).

It is important to note that the $a + A \rightarrow b + B + s$ reaction can proceed through different reaction mechanisms, besides QF, so that an investigation of the reaction mechanisms populating the $b + B + s$ final state is necessary before applying the THM formalism. In particular, the QF reaction process gives a dominant contribution to the cross section in a restricted region of the three-body phase space, where the relative momentum p_{xs} of the fragments s and x is zero (QF kinematical condition) or small compared to the bound state s-x wave number. Owing to quantum mechanics, this entails that the relative distance of x and s is very large and we can assume that s acts as a spectator to the x-A interaction, the strong interaction being short range.

Since in the THM application the A-a interaction energy is larger than E_C^{aA}, electron screening does not play a role in the reaction. Consequently, the TH cross section can be used to determine the energy dependence of the $x + A \rightarrow b + B$ S(E) down to zero relative kinetic energy without distortions due to electron screening [18,29, 30]. At low energies, where electron screening becomes important in direct measurements, the comparison between the THM astrophysical factor and direct data provides a determination of the screening potential [30–38].

In recent years, neutron induced reactions have been addressed, using deuterons as TH nuclei to transfer neutrons, while protons act as spectators [39–41]. Some of the results were included in the recent compilation of astrophysical factors of interest for nucleosynthesis and energy production in the Sun [42].

The theory of the THM for resonant and non-resonant binary sub-reactions is presented in detail in ref. [19]. In the following section the theory is shortly described.

2.1 THM: basic theory for non-resonant reactions

The first attempt to deliver the THM theory has been done by Typel, Wolter and Baur in ref. [14,15], where they introduced the surface approximation. Under such condition, only non-resonant processes (corresponding to fig. 1(a)) can be analyzed. An additional approximation used to obtain a simple factorization of the $a + A \rightarrow b + B + s$ cross section is the plane-wave approximation (PWA), which predicts reasonable energy dependence of

the $x + A \to b + B$ cross section [43] and is much simpler then the distorted wave Born approximation (DWBA) and the continuum-discretized coupled channel (CDCC) approaches. Under these conditions, the energy dependence and angular distribution of the $x + A \to b + B$ reaction are measured and normalization of THM data is obtained by scaling to direct measurements available at higher energies, where both electron screening and Coulomb suppression do not play a significant role.

In ref. [19] it has been shown that, under QF kinematical conditions, non-THM reaction mechanisms are suppressed as the terms in the reaction amplitude, containing the s-x interaction potential V_{sx} (involving the spectator s), may be small. Therefore, only the terms in the total amplitude proportional to the on-energy shell (OES) S-matrix elements can be retained. It means that QF condition has to be enforced in order to apply the THM formalism. The second important feature is that the total prior PWA amplitude is proportional to the wave function of the TH-nucleus a in momentum space, $\phi_a(\mathbf{p}_{sx})$. Therefore, the x-s momentum distribution for the system a, that is, the squared wave function in momentum space, has to be known from previous studies to extract the cross section of the $x + A \to b + B$ reaction.

As discussed at length in ref. [19] the $a+A \to b+B+s$ cross section takes the form

$$\frac{\mathrm{d}^3\sigma}{\mathrm{d}E_{c.m.}\mathrm{d}\Omega_b\mathrm{d}\Omega_B} \propto KF|\phi_a(\mathbf{p}_{sx})|^2 \left(\frac{\mathrm{d}\sigma_{xA\to bB}}{\mathrm{d}\Omega}\right)^{HOES}, \quad (2)$$

where KF is a kinematical factor, function of the masses m_i , momenta k_i and angles θ_i of the outgoing particles (see [44] for its explicit expression). The momentum distribution $|\phi_a(\mathbf{p}_{sx})|^2$ is usually described in terms of Hänkel, Eckart or Húlthen functions depending on the $x-s$ system properties [45]. $(\frac{\mathrm{d}\sigma}{\mathrm{d}\Omega})_{(xA\to bB)}$ is the half off-energy-shell (HOES) differential cross section of the $x + A \to b + B$ reaction; it is referred to as HOES as in the entrance channel x is off-energy shell, while particles in the exit channel are all fulfilling the mass-shell equation. The HOES cross section approaches the OES one only when the beam energy in the x-A center of mass is much larger than the x-s binding energy. In other cases, corrections have to be introduced. In the case $E_{c.m.}$ approaches zero energy, which is the most interesting case for astrophysics, the main correction factor is the penetrability factor $P_l(k_{xA}r_{xA})$, whose absence in the THM formalism makes it possible to extend the measurement of the binary cross section down to astrophysical energies. In the case of neutron-induced reactions ($x = n$), where the Coulomb barrier is obviously absent in the entrance channel, if the $n+A \to b+B$ reaction occurs with $l > 0$, only the centrifugal barrier plays a role and has to be introduced before comparing the THM cross section with the direct one [39–41].

2.2 Basic theory of resonant reactions

Resonant reactions play a key role in astrophysics as the appearance of resonances in the astrophysical factor might determine a dramatic change in the reaction rate, if resonances sit at energies of astrophysical interest. For instance, in the case of branch-point reactions (such as the $^{15}\mathrm{N}(p,\alpha)^{12}\mathrm{C}$ reaction [46–48]), the relative weight of the different branches can be strongly affected by low-energy resonances thus significantly changing the resulting isotopic abundance pattern.

A peculiar role is played by broad sub-threshold resonances, if they are broad enough to have a tail extending to energies above the threshold. The THM in its formulation for resonant reaction has proven an invaluable tool to investigate resonances both above and below the threshold.

Figure 1(b)) describes a QF process occurring through the formation of a compound system F. Following [19,49–51], under the non-essential hypothesis that the nucleus a undergoing breakup is at rest in the laboratory system, the x-A relative energy can be written in terms of energy and momenta of the intervening particles:

$$E_{x\text{-}A} = \frac{m_x}{m_x + m_A}E_A - \frac{p_s^2}{2\mu_{sF}} + \frac{\mathbf{p}_s \cdot \mathbf{p}_A}{m_x + m_A} - \varepsilon_{sx}, \quad (3)$$

where m_i, $\mathbf{p}_i$ and E_i are the mass, momentum and energy of the i-th particle, μ_{sF} the s-F reduced mass and ε_{sx} the x-s binding energy. Therefore, negative $E_{x\text{-}A}$ energies can the explored by choosing a suitable combination of beam energy, spectator momentum and target nucleus a. Indeed, in a number of cases the same participant x can be transferred off different targets a, each contributing to eq. (3) with a specific binding energy ε_{sx}.

Starting with the PWA in the prior form and neglecting, for simplicity, the spins of the particles involved in the reaction, the amplitude of the $a+A \to b+B+s$ takes the form

$$M^{PWA(\mathrm{prior})}(P,\mathbf{k}_{aA}) = \langle \chi^{(0)}_{sF}\Psi^{(-)}_{bB}|V_{xA}|\varphi_a\varphi_A\chi^{(0)}_{aA}\rangle, \quad (4)$$

where $P = (\mathbf{k}_{sF}, \mathbf{k}_{bB})$ is the six-dimensional momentum describing the three-body system s, b and B. $\chi^{(0)}_{aA} = \exp(i\mathbf{k}_{aA}\cdot\mathbf{r}_{aA})$, $\chi^{(0)}_{sF} = \exp(i\mathbf{k}_{sF}\cdot\mathbf{r}_{sF})$, $\mathbf{r}_{ij}$ and $\mathbf{k}_{ij}$ are the relative coordinate and relative momentum of nuclei i and j, $\Psi^{(-)}_{bB}$ is the wave function of the fragments b and B in the exit channel, $F = b + B$, V_{xA} is the interaction potential of x and the target nucleus A, φ_a and φ_A are the bound state wave functions of nuclei a and A, respectively.

If the direct coupling between the initial $x + A$ and final $b + B$ channels is neglected, that is, if we assume that resonant reaction mechanism is dominant, the wave function $\Psi^{(-)}_{bB}$ can be conveniently expressed using the spectral decomposition given by ref. [52]. This leads to the shell-model based resonant R-matrix representation for $\Psi^{(-)}_{bB}$ which is similar to the level decomposition of the wave function in the internal region in the R-matrix approach:

$$\Psi^{(-)}_{bB} \approx \sum_{\nu,\tau=1}^{N} \tilde{V}_{\nu\, bB}(E_{bB})\,[\mathbf{A}^{-1}]_{\nu\tau}\,\Psi_\tau. \quad (5)$$

Here N is the number of the levels included, E_{bB} is the relative kinetic energy of nuclei in the channel $b+B$, Ψ_τ is

the bound-state wave function describing the compound system F excited to the level τ. $\mathbf{A}_{\nu\tau}$ is the same level matrix as in the conventional R-matrix theory and is given by ref. [52]. It depends on the entry and exit channels reduced width amplitudes, energy levels and energy shifts. It means that reduced width amplitudes and level energies can be obtained from the fitting of the experimental THM cross section and used to deduce the $A(x,b)B$ astrophysical factor, since they are the same in both THM and direct data [49,53–55].

In the PWA, a formula simular to eq. (2) is found; however, the a-A and the s-F interactions can be treated as well within the distorted waves (DWBA) or the more advanced CDCC formalism [53]. This is very important as it opens the possibility to make normalization to direct data, at present a major drawback of THM especially in the investigation of reactions induced by radioactive ion beams, not necessary. A major result of the THM formalism for resonant reactions is that the factor $P_l^{-1/2}(k_{xA}, R_{xA})$ explicitly appears in the equations, eliminating the penetrability factor in the $x + A$ channel.

In the case of the THM measurement of a subthreshold state, the ANC can be deduced, clearly disclosing the deep connection of the two indirect approaches [49, 55].

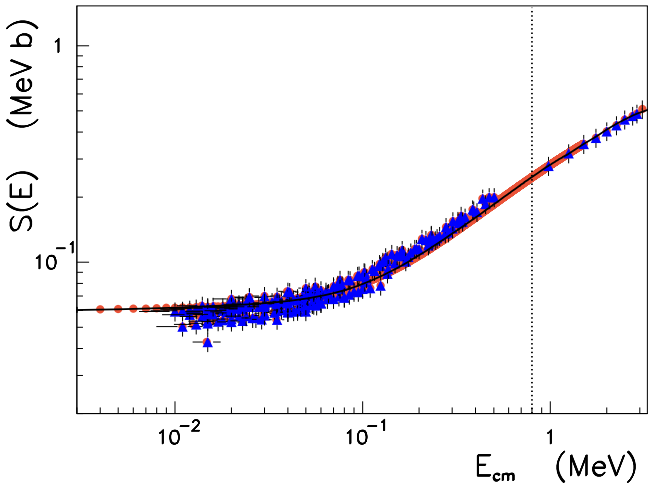

Fig. 2. ^{2}H$(d,p)^3$H S-factor measured with direct methods, blue solid triangles (only data above 10 keV were considered in order to get rid of the electron screening enhancement) and with the Trojan Horse Method (red solid circles) [32,34]. The solid line is an R-matrix fit [57]. The vertical dotted line marks the upper value of the energy range of interest for primordial nucleosynthesis.

3 Application of THM: New results in the case of non-resonant reactions

3.1 The ^{2}H(d, p)^{3}H and ^{2}H(d, n)^{3}He reactions

Over the last decades, Big Bang nucleosynthesis (BBN) has emerged as one of the founding stones of the Big Bang, joining the Hubble expansion and the cosmic microwave background radiation (CBR) in this role. Among them, Big Bang nucleosynthesis probes the Universe to the earliest times, from a fraction of a second to hundreds of seconds. Since BBN involves events that occurred at temperature of order of 1 MeV, it naturally plays a key role in forging the natural connection between cosmology, particle physics and nuclear physics. BBN nucleosynthesis requires several nuclear physics inputs and, among them, an important role is played by nuclear reaction rates. Due to the relatively small amount of key nuclear species involved in the BBN nuclear reaction network, only 12 reactions play a major role [56].

An experimental program has been carried out during the last decade to apply the THM to study several reactions selected among those of relevance for the BBN, *e.g.* ^{2}H$(d,p)^3$H, ^{2}H$(d,n)^3$He, ^{7}Li$(p,\alpha)^4$He and ^{3}He$(d,p)^4$He. In particular, the d+d cross section has been extensively measured in laboratory for both the *mirror channels* ^{2}H$(d,p)^3$H and ^{2}H$(d,n)^3$He.

Recently, a review of existing data has been performed to recommend a set of reaction rates to be used in BBN calculations [57]. Considering only results with a center-of-mass energy of interest for BBN (*i.e.* around 1 MeV), the choice of direct data has been done selecting the newest and most reliable data sets, taking into account the possible presence of systematic errors.

For ^{2}H$(d,p)^3$H, the ones reported in [58–65] and the most recent result from [66] were chosen. The data set of [58] reaches down to a center-of-mass energy value of 1.62 keV, but at such low energies a clear enhancement due to the electron screening effect is present. Thus, in order to be used for astrophysical applications, they needed to be corrected for this effect. It is also noticeable that the energy range between 600 keV and 1 MeV is not covered by any data set, making it difficult to provide a reliable fit in the whole energy range.

The Trojan Horse experiment for this channel has been performed in two runs by measuring the three-body reaction ^{2}H$(^3$He$, pt)^1$H. The data analysis has been performed according to the THM prescriptions after selection of the QF mechanism and has allowed to measure the bare nucleus S-factor in the whole energy range from 2.6 keV up to 1.5 MeV, with a 5% error (a full review is given in [32–34]). This has allowed us to have measurements for this cross section also in the energy range 0.5–1 MeV where no direct data were available. THM data have been normalized to direct ones above 1 MeV. THM data have been also extracted from the ^{2}H$(^6$Li$, pt)^4$He reaction (after ^{6}Li break-up) as reported in [67]. The electron screening potential has also been extracted for the ^{2}H$(d,p)^3$H reaction and a value of 13.4 $\pm$0.6 eV has been found (which is in agreement with the adiabatic limit [68] $U_{ad} = 14$ eV). In fig. 2 the S-factor for the reaction ^{2}H$(d,p)^3$H is shown. This has been obtained with the THM (red filled circles) and by the different direct measurements (blue triangles) cited above. The solid line is an R-matrix fit to both direct and indirect data.

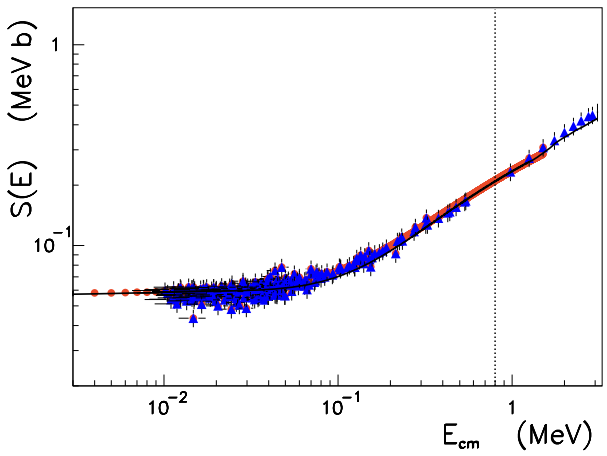

Fig. 3. Same as fig. 2, but for the ^{2}H$(d,n)^3$He reaction.

The *status of the art* before the THM measurement of the ^{2}H$(d,n)^3$He is very similar to its mirror channel.The most relevant data sets in the energy range between 600 keV and 1 MeV are missing and, in addition, no experimental point below 6 keV is present. For this reason, the direct data from references [58–66,69–73] were used for our fit. The bare nucleus S-factor has been obtained from the ^{2}H(^{3}He, n^3He)^{1}H by means of the THM [32,34], and is shown in fig. 3. The spectator particle detection technique has been adopted to avoid all the experimental problems related to neutron detection. A 5% experimental error on the whole data set, from 2.6 keV up to 1.5 MeV has been obtained. As for the other channel, THM allowed to measure the $S(E)$-factor in the 0.5–1 MeV energy range. Then, a R-matrix fit has been performed over THM and direct measurements from [57,58,60,63–65,69–73] and is shown as a solid line in fig. 3, together with the experimental points.

3.2 The ^{7}Li(p, α)^{4}He reaction

Besides its importance in the BBN, the ^{7}Li$(p,\alpha)^4$He plays an important role in stellar nucleosynthesis as it is a major lithium burning process in stars. In detail, the attempt to solve the long standing "lithium problem", *i.e.* the inability of current stellar models to predict the observed surface lithium abundance, has triggered several theoretical works.

The "lithium problem" is part of the larger field of investigation, usually referred to as "light element depletion", involving beryllium and boron as well [36,74,75].

The ^{7}Li$(p,\alpha)^4$He reaction has been studied [29] via the THM application to the QF ^{2}H$(^7$Li$,\alpha\alpha)n$ reaction, by using deuteron as TH-nucleus [76]. The same reaction has been studied also by using ^{3}He as TH-nucleus [77]. By selecting only the experimental events corresponding to neutron momentum values lower than 40 MeV/c, it was possible to span both the energy region of astrophysical importance and the energy region where direct data not affected by electron screening are available. In this way, THM data were normalized to the direct measurements

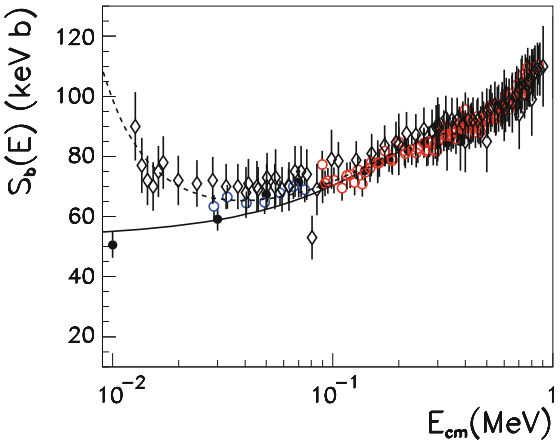

Fig. 4. The THM ^{7}Li$(p,\alpha)^4$He $S(E)$-factor (black points) discussed in ref. [81], normalized to the direct data [79,80] (blue and red circles, respectively). The full black line describes the bare-nucleus $S_b(E)$-factor while the dashed one describes the enhancement of the direct data of Engstler *et al.* [78] due to electron screening leading to $U_e = 425 \pm 60$ eV.

of ref. [78], obtaining a zero-energy S-factor $S_b(0) = 55 \pm 3$ keV barns. Recently, taking advantage of the more recent ^{7}Li$(p,\alpha)^4$He direct measurements of ref. [79,80], a new normalization procedure has been applied in ref. [81] for the same THM data discussed in ref. [29]. Normalization has been performed at energies ranging from 200 keV up to 400 keV with an evaluated error of $\sim$ 4%. The result obtained in the analysis of ref. [81] is reported in fig. 4, where the THM data (black points) are compared with the ones of ref. [79] and ref. [80] (blue and red circles, respectively) and those of ref. [78] (open diamonds). The full black line represents the fit of the THM bare-nucleus $S_b(E)$-factor, via a second order polynomial function

$$S_b(E) = 53 + 213 \cdot E - 336 \cdot E^2 \text{ keV barns}, \qquad (6)$$

where the energy E is expressed in MeV. The fit yields to the value of $S_b(0) = 53 \pm 5$ keV barns, where the evaluated error takes into account a $\sim$ 4% uncertainty related to the normalization procedure, a $\sim$ 6% uncertainty related to statistics and a further uncertainty of $\sim$ 6% related to the errors affecting the direct data of ref. [80] (on the average).

In fig. 4, the low-energy ($<$ 60 keV) direct data of refs. [78,79] has then been fitted leaving U_e as the only free parameter and taking eq. (6) as the bare nucleus S-factor. This procedure leads to the value of $U_e = 425 \pm 60$ eV, where the quoted error takes into account a $\sim$ 14% contribution related to the uncertainties in the low-energy direct data of [78].

The bare-nucleus $S_b(E)$-factor of eq. (6) have then been used for evaluating the ^{7}Li$(p,\alpha)^4$He reaction rate in the temperature range of $0.01 < T_9 < 2$. Its ratio to the NACRE one is shown in fig. 5, where a discrepancy ranging from $\sim$ 13% at $T_9 = 10^{-3}$ to $\sim$ 5% at $T_9 = 1$ is clearly visible. The impact of such discrepancy has been evaluated in ref. [83] in the framework of Red Giant Branch (RGB) nucleosynthesis by means of the theoretical astrophysical models discussed in ref. [84,85]. In particular, it

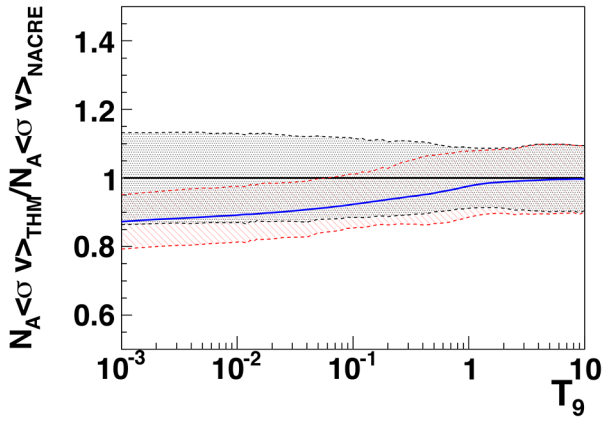

Fig. 5. Ratio between the THM ^{7}Li$(p,\alpha)^4$He reaction rate and the NACRE one [82] (full blue line), together with THM upper and lower limits (red dashed lines) [81]. This is compared with the upper and lower values recommended in NACRE (black dashed lines).

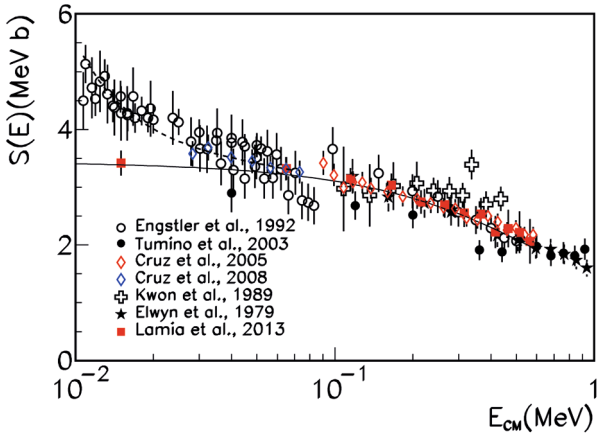

Fig. 6. The THM $S(E)$-factor of ref. [83] for the ^{6}Li$(p,\alpha)^3$He reaction (red squares) normalized to the ones of ref. [80,82]. The TH data from [86] are reported as black points. The full line is the bare nucleus $S_b(E)$-factor as given in eq. (6), while the dashed line describes the enhancement due to the electron screening, taking an electron screening potential $U_e = 355 \pm 100$ eV.

has been found that the understanding of the ^{7}Li abundance in RGB is strongly influenced by the uncertainty affecting mixing phenomena, while the uncertainty connected with the reaction rate is negligible.

3.3 The THM ^{6}Li(p, α)^{3}He study

The ^{6}Li$(p,\alpha)^3$He reaction has been studied via the THM applied to the ^{2}H$(^6$Li$,\alpha^3$He$)n$ QF reaction, as discussed in details in refs. [86,87]. By normalizing THM data to the direct measurement of ref. [78], we got $S(0) = 3.00 \pm 0.19$ MeV barns, where the quoted error is only the statistical one, while an additional $\sim 11\%$ error is due to the normalization procedure to the direct data [78]. A further THM measurement has been later performed for exploring the energy range $\sim$ 10–400 keV [88].

Recently, the work of ref. [83] reanalyzes the same THM data of refs. [88] in the light of the recent direct measurements in refs. [79,80]. In particular, the high-energy data of ref. [80], affected by an overall error of about $\sim 6\%$, together with the direct measurements collected in the NACRE compilation [82], have been used to normalize the THM data. The result of this new data analysis given in ref. [83] is reported in fig. 6, where the THM data are reported as full red-squares while the full-black points represent the THM data of [86]. The full black line is the fit of the THM bare nucleus $S_b(E)$-factor, given by

$$S_b(E) = 3.44 - 3.50 \cdot E + 1.74 \cdot E^2 + 0.23 \cdot E^3 \text{ MeV barns}, \quad (7)$$

where E is given in MeV. This leads to the value of $S_b(0) = 3.44 \pm 0.35$ MeV barns, where the total error accounts for the statistical error on the TH experimental points ($\sim 7\%$ on the average), on the direct data ($\sim 7\%$ on the average) and on the normalization procedure ($\sim 3\%$). In fig. 6, the dashed line describes the enhancement of the $S(E)$-factor for the low-energy direct data and it has been obtained by fitting the direct data in refs. [78,79], adopting the bare nucleus $S_b(E)$-factor of eq. (7). The procedure leads to the value of $U_e = 355 \pm 100$ eV.

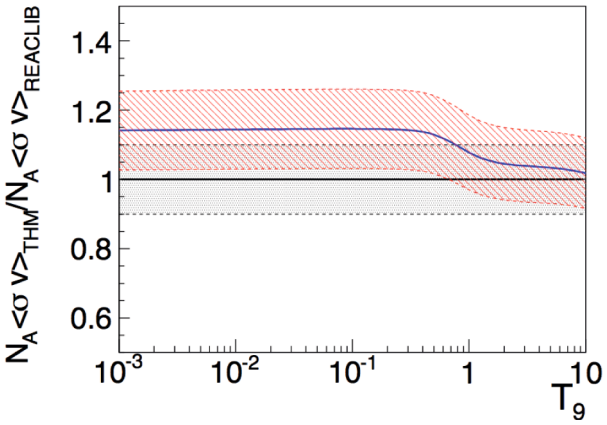

Fig. 7. Ratio between the THM ^{6}Li$(p,\alpha)^3$He reaction rate and the REACLIB one [89] (full blue line), together with THM upper and lower limits (red dashed lines) [83]. The black dashed area gives the upper and lower limits of the REACLIB reaction rate assuming the same uncertainties reported in the NACRE compilation of ref. [82].

Then, the obtained THM reaction rate has been compared with the one reported in the JINA REACLIB library [89] and the result is reported in fig. 7. The effect of the $\sim 15\%$ discrepancy at temperatures lower than 10^8 K has been evaluated in Pre-Main Sequence (PMS) stars by means of the updated FRANEC code [90–92]. The ^{6}Li temporal evolution has been studied for different stellar masses and metallicities. It has been found that the uncertainties in the adopted reaction rate hardly influence the stellar physics with respect to other input parameters (such as helium abundance, metallicity, opacity, ...).

4 Application of THM: New results in the case of resonant reactions

4.1 The ^{19}F(p, α)^{16}O reaction: The case of resonances above threshold

Understanding fluorine production in Asymptotic giant branch (AGB) stars [93] may lead to a more accurate picture of heavy element nucleosynthesis through the s-process [94]. The $^{19}\mathrm{F}(p,\alpha)^{16}\mathrm{O}$ channel is the main fluorine depleting reaction in hydrogen rich environments, such as the outer layers of AGB stars [95]. However, only a direct data set is available at energies $E_{c.m.} \leq 300$ keV [96], where fluorine burning is most effective, in particular for the α_0 channel, corresponding to the emission of α-particles off ^{20}Ne leaving ^{16}O in its ground state, which is regarded as the main contributing channel [97]. However, Lombardo *et al.* data [96] stop at 200 keV and the lowest data points are affected by a considerable uncertainty.

While refs. [96,98] indicate the existence of resonances at $E_{c.m.} \leq 0.4$ MeV, the unpublished data of [99] and the NACRE extrapolation support a non-resonant trend of the low-energy $S(E)$ factor. This contradiction and the very simple recommended extrapolation to astrophysical energies have generated speculations about a nuclear origin of the discrepancies observed in Galactic fluorine studies [54], since the largest observed fluorine overabundances cannot be explained with standard AGB models including extra-mixing (see [100], for instance). This has requested a reassessment of the nuclear reaction rates involved in fluorine production and destruction.

Since the astrophysical factor shows a definitely resonant behavior above 0.6 MeV, the THM in its modified version developed to handle resonant reactions is very suitable to investigate the $^{19}\mathrm{F}(p,\alpha)^{16}\mathrm{O}$ astrophysical factor. To this purpose, THM was applied to the $^{2}\mathrm{H}(^{19}\mathrm{F},\alpha^{16}\mathrm{O})n$ reaction. Details on the experimental setup and the analysis procedures are given in [54]. This work showed the occurrence of a peak at 113 keV, sitting inside the Gamow window, which was not observed before and might have important consequences for astrophysics. The p-^{19}F relative energy spectrum spanned an energy interval from 0 to about 1 MeV, making it possible to normalize the THM astrophysical factor to the existing direct data. Recently, the data from ref. [54] have been reanalyzed [101] to evaluate the influence of the new improved direct data at high energy by Lombardo *et al.* [102].

Figure 8 shows the $S(E)$-factor calculated with the resonance parameters from the fitting of THM data below 600 keV. Above this energy, the resonance parameters are taken from the fitting of the data from ref. [102] for normalization. Since the THM cross section yielded the resonance contribution only, the non-resonant part of the cross section was taken from ref. [82]. The middle red curve marks the $S(E)$-factor computed using the parameters from the best fit, while the red band arises from the uncertainties on the resonance parameters, due to the combined statistical, normalization and energy shift errors (including correlation). An average error of 20% was obtained. At present, the main source of uncertainty is due to the non-resonant contribution to the astrophysical factor, since the one given in [82] is based on a very simple calculation.

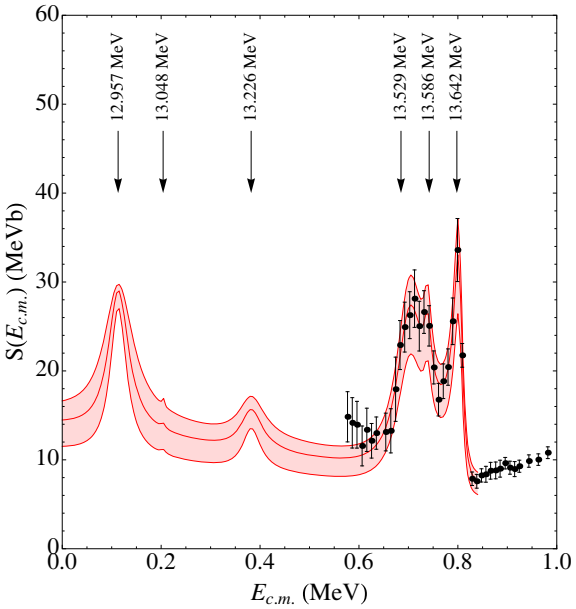

Fig. 8. THM astrophysical factor of the $^{19}\mathrm{F}(p,\alpha_0)^{16}\mathrm{O}$ reaction, normalized to the data from [102] above 600 keV, as shown in [101]. The middle red line marks the recommended S-factor, while the upper and lower red lines stand for upper and lower limits set by combining statistical, normalization and energy shift error. The solid symbols represent the direct astrophysical factor in [102]. Finally, the arrows mark the ^{20}Ne states contributing to the $S(E)$-factor.

4.2 The ^{13}C(α, n)^{16}O reaction: The case of sub-threshold resonances

A key reaction for understanding the s-process is the $^{13}\mathrm{C}(\alpha,n)^{16}\mathrm{O}$. In AGB stars, ^{13}C nuclei give up their excess neutrons to heavier nuclei through the $^{13}\mathrm{C}(\alpha,n)^{16}\mathrm{O}$ reaction, at temperatures varying between $0.8\cdot10^8$ K and $1\cdot10^8$ K [103]. At $0.9\cdot10^8$ K, the energy range where the $^{13}\mathrm{C}(\alpha,n)^{16}\mathrm{O}$ reaction is most effective, the Gamow window [104], is $\sim$ 140–230 keV.

However, direct measurements could reach the lowest energy of $\sim$ 280 keV [105]; lower energies cannot be reached with present-day facilities owing to the strong suppression of the cross section due to the Coulomb penetration factor. Moreover, at these energies the astrophysical factor has to be corrected for atomic electron screening. Therefore, extrapolation has been performed, mostly using the R-matrix approach; the most recent result [106] reports a 100 keV astrophysical factor $S(100\,\mathrm{keV}) = 3.3^{+1.8}_{-1.4}\times10^6$ MeV barns.

On the other hand, indirect measurements aimed at deducing the ANC or the spectroscopic factor of the 6.356 MeV level in ^{17}O through α-transfer reactions (see [49] for a review of the indirect measurements). However, contradicting values of the ANC and of the

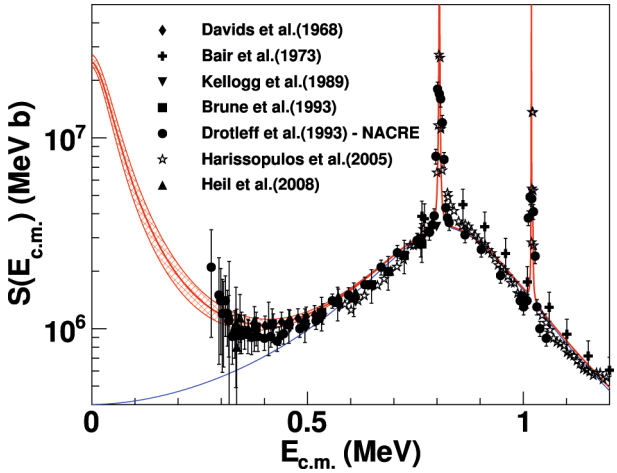

Fig. 9. R-matrix calculated $S(E)$-factor (red middle line), obtained using the THM resonance parameters below $E_{c.m.} = 500$ keV and the parameters from ref. [106] above, from ref. [49]. The upper and lower red lines mark the range allowed by experimental errors affecting THM data and by the normalization uncertainty. The R-matrix $S(E)$-factor not including the subthreshold resonance at -3 keV is displayed with a blue line. Black symbols are used for direct data normalized as in [106]. Different symbols are used for each data set, as specified in the inset. See ref. [49] for more details.

spectroscopic factors were obtained. Moreover, systematic errors might be introduced, especially in the case of the extraction of the spectroscopic factor. Theoretical calculations were also performed [107,108].

To summarize, an untenable spread in the values of the low-energy S-factor is present, ranging from 1.2×10^6 [109] to 6.3×10^6 MeV barns [110] at a reference center-of-mass energy of 100 keV. The THM is well suited to investigate the ^{13}C$(\alpha, n)^{16}$O process, as it allows to explore the negative energy region and, consequently, to observe the -3 keV peak. Therefore, we used ^{6}Li, having a well-known $\alpha + d$ structure, to transfer an α-particle to ^{13}C while d was emitted without interacting in QF kinematics. ^{16}O from the ^{13}C$(\alpha, n)^{16}$O sub-reaction and deuterons were detected, to maximize the detection efficiency and reduce systematic uncertainties. Figure 9 shows the THM S-factor (red band), compared with direct data in the literature (black symbols). The blue line demonstrates how the S-factor would look like in the case the -3 keV peak was not present. More details on fig. 9 are given in ref. [49].

The THM S-factor is obtained by taking the resonance reduced widths from the THM cross section of the ^{13}C$(^6$Li$, n^{16}$O$)^2$H QF process. Normalization was obtained by scaling the resonance parameters to those of the peaks above $\sim$ 500 keV; to have a robust normalization and minimize normalization errors, the contribution of the resonances up to about 1.2 MeV was considered in the normalization procedure. The THM astrophysical factor agrees, within uncertainties, with existing extrapolations of the ^{13}C$(\alpha, n)^{16}$O S-factor to the Gamow window, with theoretical calculations and other indirect approaches, taking into account possible sources of systematic errors. The THM results, however, seem to indicate that the largest values of the extrapolated S-factor are preferable. The most striking result is a significant reduction of the uncertainty affecting the ^{13}C$(\alpha, n)^{16}$O S-factor at the Gamow peak, which is reduced from about 50% to about 20%. As a result of the THM measurement, preliminary astrophysical calculations have shown that a different neutron density and flux might modify the relative abundances of isotopes placed in correspondence of branching points and could be crucial for an accurate determination of the solar element distribution [49]. Detailed study of the effects of the new, improved ^{13}C$(\alpha, n)^{16}$O reaction rate are under examination, extending the astrophysical analysis to different stellar models of low-mass AGB stars.

5 Final remarks

In this review, we have focused on the THM indirect technique that has been used extensively for determining reaction rates in nuclear astrophysics. The theoretical description of this technique has been presented and a review of its use in the case of both resonant and non-resonant reactions, as well as astrophysical implications, has been given. This method is now a well established tool in nuclear astrophysics. As rare isotope beam facilities are being developed around the world, the THM will play a major role in determining rates for reactions that occur on short-lived isotopes. The work that has been done to date with rare-isotope beams represents only the first step in this effort [111,112]. Beam intensities and beam species will expand dramatically by the end of this decade opening up many new opportunities to further utilize the THM to learn about the nuclear reactions that drive the cosmos.

References

1. E.M. Burbidge, G.R. Burbidge, W.A. Fowler, F. Hoyle, Rev. Mod. Phys. **29**, 547 (1957).
2. W.A. Fowler, Rev. Mod. Phys. **56**, 149 (1984).
3. C. Rolfs, W.S. Rodney, *Cauldrons in the Cosmos* (University of Chicago Press, Chicago, 1988).
4. C. Rolfs, Prog. Part. Nucl. Phys. **46**, 23 (2001).
5. R. Bonetti *et al.*, Phys. Rev. Lett. **82**, 5205 (1999).
6. H.J. Assenbaum, K. Langanke, C. Rolfs, Z. Phys. A **327**, 461 (1987).
7. F. Strieder, C. Rolfs, C. Spitaleri, P. Corvisiero, Naturwissenschaften **88**, 461 (2001).
8. G. Baur, C.A. Bertulani, H. Rebel, Nucl. Phys. A **458**, 188 (1986).
9. A.M. Mukhamedzhanov *et al.*, Phys. Rev. C **56**, 1302 (1997).
10. A.M. Mukhamedzhanov, R.E. Tribble, Phys. Rev. C **59**, 3418 (1999).
11. G. Baur, Phys. Lett. B **178**, 135 (1986).
12. C. Spitaleri, in *Problems of Fundamental Modern Physics, II: Proceedings*, edited by R. Cherubini, P. Dalpiaz, B. Minetti (World Scientific, 1991) p. 21.
13. S. Cherubini *et al.*, Astrophys. J **457**, 855 (1996).

14. S. Typel, H. Wolter, Few-Body Syst. **29**, 75 (2000).
15. S. Typel, G. Baur, Ann. Phys. (N.Y.) **305**, 228 (2003).
16. A.M. Mukhamedzhanov *et al.*, Eur. Phys. J. A **27, Suppl. 1**, 205 (2006).
17. A.M. Mukhamedzhanov *et al.*, J. Phys. G **35**, 014016 (2008).
18. C. Spitaleri *et al.*, Phys. At. Nucl. **74**, 1725 (2011).
19. R.E. Tribble *et al.*, Rep. Prog. Phys. **77**, 106901 (2014).
20. I.S. Shapiro, Usp. Fiz. Nauk **92**, 549 (1967).
21. I.S. Shapiro *Interaction of high-energy particles with nuclei International School of Physics Enrico Fermi*, Course 38, edited by E.O. Ericson (Academitices, New York, 1967) p. 210.
22. I.S. Shapiro, Sov. Phys. Usp. **10**, 515 (1968).
23. G.F. Chew, G.C. Wick, Phys. Rev. **85**, 636 (1952).
24. M. Furic *et al.*, Phys. Lett. B **39**, 629 (1972).
25. M. Lattuada *et al.*, Nucl. Phys. A **458**, 493 (1986).
26. M. Zadro *et al.*, Phys. Rev. C **40**, 181 (1989).
27. G. Calvi *et al.*, Phys. Rev. C **41**, 1848 (1990).
28. A. Tumino *et al.*, Phys. Rev. C **78**, 064001 (2008).
29. M. Lattuada *et al.*, Astrophys. J. **562**, 1076 (2001).
30. C. Spitaleri *et al.*, Phys. Rev. C **63**, 055801 (2001).
31. M. La Cognata *et al.*, Phys. Rev. C **72**, 065802 (2005).
32. A. Tumino *et al.*, Phys. Lett. B **700**, 111 (2011).
33. A. Tumino *et al.*, Phys. Lett. B **705**, 546 (2011).
34. A. Tumino *et al.*, Astrophys. J. **785**, 96 (2014).
35. Q. Wen *et al.*, Phys. Rev. C **78**, 035805 (2008).
36. L. Lamia *et al.*, J. Phys. G **39**, 015106 (2012).
37. M.L. Sergi *et al.*, Phys. Rev. C **91**, 065803 (2015).
38. C. Spitaleri *et al.*, Phys. Rev. C **90**, 035801 (2014).
39. A. Tumino *et al.*, Eur. Phys. J. A **25**, 649 (2005).
40. M. Gulino *et al.*, J. Phys. **37**, 125105 (2010).
41. M. Gulino *et al.*, Phys. Rev. C **87**, 012801(R) (2013).
42. E.G. Adelberger *et al.*, Rev. Mod. Phys. **83**, 195 (2011).
43. E.I. Dolinsky *et al.*, Nucl. Phys. A **202**, 97 (1973).
44. C. Spitaleri *et al.*, Phys. Rev. C **69**, 055806 (2004).
45. R.G. Pizzone *et al.*, Phys. Rev. C **80**, 025807 (2009).
46. M. La Cognata *et al.*, Eur. Phys. J. A **27**, S1, 249 (2006).
47. M. La Cognata *et al.*, Phys. Rev. C **76**, 065804 (2007).
48. M. La Cognata *et al.*, Phys. Rev. C **80**, 012801 (2009).
49. M. La Cognata *et al.*, Astrophys. J. **777**, 143 (2013).
50. M. La Cognata *et al.*, Astrophys. J. **723**, 1512 (2010).
51. M. La Cognata *et al.*, J. Phys. G **35**, 014014 (2008).
52. C. Mahaux, H.A. Weidenmüller, *Shell- Model Approach to Nuclear Reactions* (North-Holland Publishing Company, Amsterdam 1969).
53. A.M. Mukhamedzhanov *et al.*, Phys. Rev. C **83**, 044604 (2011).
54. M. La Cognata *et al.*, Astrophys. J. Lett. **739**, 54 (2011).
55. M. La Cognata *et al.*, Phys. Rev. Lett. **109**, 232701 (2012).
56. E.W. Kolb, M.S. Turner, *The Early Universe* (Addison-Wesley, 1990).
57. R.G. Pizzone *et al.*, Astrophys. J. **786**, 112 (2014).
58. U. Greife *et al.*, Z. Phys. **351**, 107 (1995).
59. A. Krauss, H.W. Becker, H.P. Trautvetter, C. Rolfs, K. Brand, Nucl. Phys. A **465**, 150 (1987).
60. K.G. McNeill *et al.*, Phys. Rev. **602**, 81 (1951).
61. R.L. Schulte, Nucl. Phys. A **192**, 000 (1972).
62. N. Jarmie, R.E. Brown, Phys. Rev. C **41**, 1391 (1990).
63. A.S. Ganeev, Suppl. Sov. At. J. **5**, 26 (1957).
64. W.B. Arnold *et al.*, Phys. Rev. **483**, 93 (1954).
65. F. Raiola *et al.*, Eur. Phys. J. A **13**, 377 (2002).
66. D.S. Leonard *et al.*, Phys. Rev. C **73**, 045801 (2006).
67. R.G. Pizzone *et al.*, Phys. Rev. C **87**, 025805 (2013).
68. B. Bracci *et al.*, Nucl. Phys. A **513**, 316 (1990).
69. V.A. Davidenko *et al.*, J. Nucl. Energy **258**, 2 (1957).
70. M.A. Hofstee *et al.*, Nucl. Phys. A **688**, 527 (2001).
71. A.S. Belov *et al.*, Nuovo Cimento A **103**, 1647 (1990).
72. N. Ying *et al.*, Nucl. Phys. A **481**, 206 (1973).
73. V.M. Bystritsky *et al.*, Izv. Rossiiskoi Akad. Nauk. **563**, 74 (2010).
74. S. Romano *et al.*, Eur. Phys. J. A **27**, 221 (2006).
75. L. Lamia *et al.*, Nuovo Cimento C **31**, 423 (2008).
76. L. Lamia, M. La Cognata, C. Spitaleri, B. Irgaziev, R.G. Pizzone, Phys. Rev. C **85**, 025805 (2012).
77. R.G. Pizzone *et al.*, Phys. Rev. C **83**, 045801 (2011).
78. S. Engstler *et al.*, Phys. Lett. B **20**, 279 (1992).
79. J. Cruz *et al.*, Phys. Lett. B **624**, 181 (2005).
80. J. Cruz *et al.*, J. Phys. G **35**, 014004 (2008).
81. L. Lamia *et al.*, Astron. Astrophys. **541**, 158 (2012).
82. C. Angulo *et al.*, Nucl. Phys. A **656**, 3 (1999).
83. L. Lamia *et al.*, Astrophys. J. **768**, 65 (2013).
84. S. Palmerini *et al.*, Astrophys. J. **741**, 26 (2011).
85. M. Busso *et al.*, Astrophys. J., Lett. **717**, 47 (2010).
86. A. Tumino *et al.*, Phys. Rev. C **67**, 065803 (2003).
87. R.G. Pizzone *et al.*, Astron. Astrophys. **438**, 779 (2005).
88. A. Tumino, C. Spitaleri, L. Pappalardo *et al.*, Progr. Theor. Phys. Suppl. **154**, 341 (2004).
89. R.H. Cyburt, Phys. Rev. D **70**, 023505 (2010).
90. S. Degl'Innocenti *et al.*, Astrophys. Space Sci. **316**, 25 (2008).
91. M. Dell'Omodarme *et al.*, Astron. Astrophys. **540**, A26 (2012).
92. E. Tognelli *et al.*, Astron. Astrophys. **533**, A109 (2011).
93. B.S. Meyer, Annu. Rev. Astron. Astrophys. **32**, 153 (1994).
94. F. Käppeler *et al.*, Rev. Mod. Phys. **83**, 157 (2011).
95. M. Lugaro *et al.*, Astrophys. J. **615**, 934 (2004).
96. I. Lombardo *et al.*, Phys. Lett. B **748**, 178 (2015).
97. A. Spyrou *et al.*, Eur. Phys. J. A **7**, 79 (2000).
98. G. Breuer, Z. Phys. **154**, 339 (1959).
99. H. Lorentz-Wirzba, Ph.D. thesis Universität Münster, 1978.
100. S. Lucatello *et al.*, Astrophys. J. **729**, 40 (2011).
101. M. La Cognata *et al.*, Astrophys. J. **805**, 128 (2015).
102. I. Lombardo *et al.*, J. Phys. G **40**, 125102 (2013).
103. M. Busso, R. Gallino, G.J. Wasserburg, Annu. Rev. Astron. Astrophys. **37**, 239 (1999).
104. C. Iliadis, *Nuclear Physics of Stars* (Wiley-VCH Verlag, 2007).
105. H.W. Drotleff *et al.*, Astrophys. J. **414**, 735 (1993).
106. M. Heil *et al.*, Phys. Rev. C **78**, 025803 (2008).
107. P. Descouvemont, Phys. Rev. C **36**, 2206 (1987).
108. M. Dufour, P. Descouvemont, Phys. Rev. C **72**, 01580 (2005).
109. E.D. Johnson *et al.*, Phys. Rev. Lett. **97**, 192701 (2006).
110. G.M. Hale, Nucl. Phys. A **621**, 177 (1997).
111. S. Cherubini *et al.*, Phys. Rev. C **92**, 015805 (2015).
112. R.G. Pizzone *et al.*, Eur. Phys. J. A **52**, 24 (2016).